2.2.16
WR

STATUS	TYPE	OCLC #
Submitted 20160201	Copy	931712336
SOURCE	REQUEST DATE	NEED BEFORE
ILLiad	02/01/2016	02/22/2016
BORROWER	RECEIVE DATE	DUE DATE
ALM		
LENDERS		
*UB#		

163568940

RS 6868(2013,1) ~~RQ 6889(250)~~

BIBLIOGRAPHIC INFORMATION

LOCAL ID
AUTHOR

ARTICLE AUTHOR Kandasamy, K.,

TITLE Advances in materials science for environmental and energy technologies III (Materials Science and

ARTICLE TITLE Solid-State Additive Manufacturing of Aluminum and Magnesium Alloys

IMPRINT Hoboken, NJ Wiley 2014

FORMAT Book
EDITION
VOLUME 1
NUMBER
DATE 2013
PAGES 59-69

ISBN 9781118996683 (hbk.)

SERIES NOTE (DE-601)130879606 250 25000

INTERLIBRARY LOAN INFORMATION

ALERT

AFFILIATION NAAL,ARL,ASERL,SOLINE,SO6,KUDZU
COPYRIGHT US:CCL

VERIFIED <TN:504863><ODYSSEY:206.107.44.160/ILL>
MAX COST OCLC IFM - 25.00 USD
LEND CHARGES
LEND RESTRICTIONS

SHIPPED DATE
FAX NUMBER
EMAIL

BORROWER NOTES (maxCost: 25.00)

ODYSSEY 206.107.44.160/ILL
ARIEL FTP
ARIEL EMAIL

BILL TO Gorgas Library - ILL
University of Alabama Libraries
711 Capstone Drive - Room 202
Tuscaloosa, AL, US 35487-0266

BILLING NOTES Please include the ILL number for each transaction, your FEIN, phone number, fax number and e-mail address on all invoices. Thank you.

SHIPPING INFORMATION

SHIP VIA Odyssey/Library Rate
SHIP TO Gorgas Library - ILL
University of Alabama Libraries
711 Capstone Drive - Room 202
Tuscaloosa, AL, US 35487-0266

RETURN VIA
RETURN TO

TT7

Materials Science and Technology (MS&T) 2013
October 27-31, 2013, Montreal, Quebec, Canada

Advanced Materials, Processes and Applications for Additive Manufacturing

Solid-state additive manufacturing of aluminum and magnesium alloys

Kumar Kandasamy, Liam E. Renaghan, Jacob R. Calvert, Kevin D. Creehan and Jeffrey P. Schultz
Aeroprobe Corporation, 2200 Kraft Drive, Suite #1475, Blacksburg – 24060, Virginia

Abstract

Additive friction stir (AFS) is a solid-state localized thermo-mechanical process in which wrought metal is deposited onto metallic substrates. AFS utilizes both solid and powder filler feeding for layer-wise deposition. Thus, AFS provides greater flexibility in producing components with gradient microstructure. In this study, aluminum and magnesium structures were fabricated via AFS. Microstructural and mechanical characterization was carried out to evaluate the mechanism of powder consolidation and mechanical properties. Shear-induced interfacial heating and severe plastic deformation are utilized in producing a metallurgical bond between the powder particles and layers. Compared to the current powder processing routes, AFS is more economical and energy efficient in producing near-net-shape components using advanced thermally sensitive metallic materials.

Key words: Additive friction stir, aluminum alloys, magnesium alloys, mechanical properties, powder metal consolidation

Introduction

The demand for system level performance enhancement, weight reduction and cost reduction drives materials and manufacturing innovations and research. In recent times there has been a shift in design concept from manufacturing-dependent design to performance-oriented design. This shift is attributable to innovations in manufacturing technology where more complex design can be realized at the component level. Additive manufacturing is one such manufacturing technology in fulfilling today's demands with near-net shape manufacturing. Benefits of near-net shaping are well-known in life cycle cost reduction and energy saving as the requirement for secondary processes and related tooling can be drastically reduced [1]. Particularly in the aerospace industry, the material buy-to-fly ratio is on the order of 10 to 20% where the structural weight is the main concern [2]. The lower buy-to-fly ratio is often attributed to subtractive manufacturing of webbed and ribbed components to reduce the structural weight while maintaining required stiffness. Manufacturing such components using additive manufacturing could drastically reduce the extensive machining, excessive material requirement, the associated energy requirement, the tooling, and importantly the cost, besides being eco-friendly. Layer-wise deposition/buildup in additive manufacturing gives greater flexibility in varying the chemical composition locally and in selective reinforcement with secondary phases while the parts are being manufactured [3].

Additive manufacturing technologies (at the metallic component level) can be classified into three categories based on the process principles and state of metal deposition: 1) Liquid phase additive manufacturing, 2) Spray forming, and 3) Solid phase additive manufacturing. Liquid phase additive manufacturing consists of metal deposition processes where a filler metal (in solid or powder form) is selectively sintered or melted. Selective laser sintering/melting [4], laser engineered net shaping (LENS) [5], electron beam melting [6], and arc melting (shaped metal deposition) [7] are examples of liquid phase additive manufacturing processes. While the laser-

based and electron beam-based processes are revolutionizing additive manufacturing of complex metallic parts for critical applications, they inherently result in cast microstructures. Parts produced using sintering techniques in this category require secondary densification processes. Though it is technically possible to produce large components using these power beam techniques, it is practically not viable for larger components due to the inherent process constraints and the requirement of a proportionally powerful energy source. Spray forming consists of cold [8] and thermal spray techniques [9]. While also requiring a secondary densification process, these processes require the existence of patterns onto which the coatings are formed. Though the technology readiness levels of these techniques are very well beyond the proof of concept stage, these processes are not commercially adapted or applied in these industries due to concerns over the reliability and repeatability of the physical and mechanical properties of the manufactured components.

A recent innovation to additive manufacturing technology is the solid state processes, namely ultrasonic consolidation [10], friction stir welding/processing [11], friction surfacing [12], and additive friction stir. The solid state additive manufacturing processes are thermo-mechanical processes, primarily relying on solid state bonding principles. These processes produce fully dense additive layers with wrought microstructure. Additive friction stir is a solid-state thermo-mechanical process wherein filler metal is added in the form of solid or powder. The process is schematically explained in Figure 1. The process principle is simple and similar to friction stir welding/processing, with the exception of the use of filler feed. The filler metal is forced to flow between the rotating AFS tool and the substrate, whereby the filler material undergoes shear-induced severe plastic deformation, dynamic recrystallization, and deposition, while the firmly clamped substrate is moving. The hydrostatic pressure and the heat generated from adiabatic and frictional processes are crucial in obtaining sound bonding between the substrate and filler metal.

Generically, the variable process parameters are tool geometry, spindle speed, filler feed rate, tool substrate/previous layer interference, and substrate traverse rate. The tool design has been shown to have a large impact on the deposited layer thickness, and thus the volumetric deposition rate. Tool design is the most influential parameter which controls the deposition rate. The next most significant process parameter controlling the volumetric deposition rate is the traverse rate. The maximum traverse speed for a defect-free deposition is a function of tool design, traverse rate, filler feed rate, and spindle speed. The spindle speed is the most significant parameter in controlling the temperature for a given tool; on the other hand the filler feed rate is the most significant parameter in controlling the pressure for a given tool substrate interference. The filler metal addition can be in the form of solid or powder. Continuous powder feed capability of the AFS platform allows greater flexibility in achieving functionally graded structures.

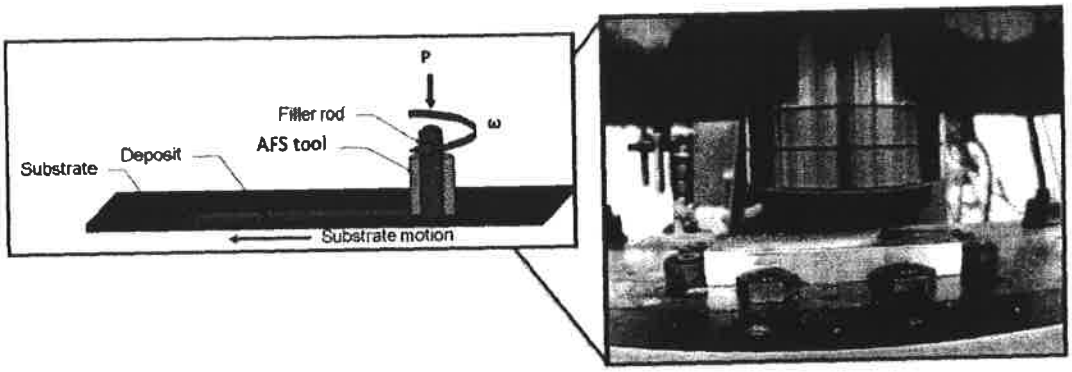

Figure 1: Schematic and pictorial representation of additive friction stir process.

In this paper we demonstrate the AFS process as an additive manufacturing process for aluminum and magnesium alloys in solid and powder form. Further, the mechanical properties of AFS deposited aluminum alloy 6061, magnesium alloy AZ31 and magnesium alloy WE43 powder are discussed.

Experimental procedure

The filler metals used in this study were solid 6061-T6 aluminum alloy, AZ31-H24 magnesium alloy, and magnesium alloy WE43 in powder form. The substrate metal used in the study for 6061-T6 deposition was 12.5mm thick cast MIC-6 (aluminum-silicon alloy) plate and the substrate metal used for magnesium alloys was 9.5mm thick AZ31B-H24 magnesium alloy plates. The process parameters used are summarized in Table 1. Powder deposition was performed by filling the tool with powder and during the process the powder is consolidated and deposited on to substrate simultaneously.

Table 1: Summary AFS process parameter used for the demonstration.

Parameter	AA6061 deposition	AZ31B deposition	WE43 powder
Tool diameter	38mm (1.5in)	38mm (1.5in)	38mm (1.5in)
Spindle speed	1000rpm	600rpm	750rpm
Traverse rate	76mm/min(3in/min)	51mm/min (2in/min)	25.4mm/min (1inch/min)
Filler feed rate	38mm/min (1.5in/min)	25mm/min (1in/min)	15mm/min (0.6in/min)
Layer thickness	1.4mm (0.055in)	0.8mm (0.033in)	0.5mm (0.02in)
Filler metal	AA6061-T6	AZ31B-H24	Ground WE43 powder
Substrate	MIC-6	AZ31B-H24	AZ31B-H24

After deposition metallographic samples and tensile testing samples were machined to analyze the integrity of the additively manufactured structures. Orientation of the tensile samples extracted from 6061 and AZ31 solid deposited samples are shown in figure 2. For the WE43 powder deposit the tensile samples were taken from the transverse direction. The dimensions of miniaturized tensile samples were 10mm in gage length, 2.5mm in width and 1.5mm in thickness, and Vickers micro hardness testing parameters were 200g force and 10s dwell time.

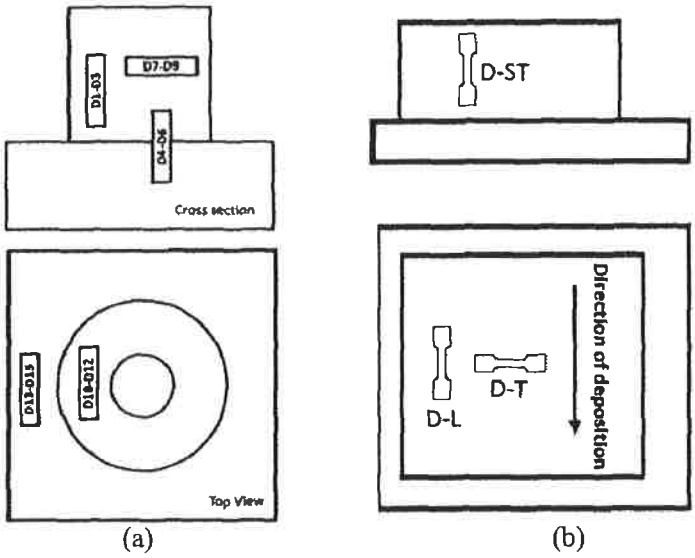

(a) (b)

Figure 2: Orientation of tensile samples extracted from (a) AA6061 deposit, and b) AZ31 deposit. (L-Longitudinal, T-Transverse and ST-Short transverse).

Result and discussion

a) Deposition of AA6061 and AZ31 using solid filler metal

Figure 3 shows the photographs of an AFS-manufactured aluminum 6061 ring on cast MIC-6 plate and an AZ31 magnesium block on a similar substrate. The size of the aluminum ring was 89mm outer diameter, 51mm inner diameter and 25mm height (3.5" OD, 2" ID and 1" height). The size of the AZ31 block deposited was 152 mm x 127 mm x 25 mm (6" long x 5" wide x 1" thick).

Figure 4 shows the cross section macrostructure of the AFS aluminum ring wall and Mg block, which shows defect-free deposits with full density. The density measurements also show that there are no volumetric defects in the deposit and the density is equal to the parent metal density. The layer wise deposition is evident from the macrostructure. The layer-wise deposition allows us to change the local composition and constituents. Thus, the main advantage of the AFS process is that the layer thickness and volume fraction can be dynamically changed.

Figure 5 shows the hardness profile along the thickness direction across the substrate/deposit interface. In AA6061 deposit the MIC-6 substrate is harder than the deposit. The hardness profile shows that the deposit getting softened upon multiple thermal exposure. This can be inferred from a gradual decrease in hardness along the thickness from top layer for few layers. After a certain number of thermal exposures the maximum harness of 58VHN decreases to 42VHN and stabilizes. In the AZ31 deposit, it is evident from the hardness profile that the deposit prepared from the similar base metal (57VHN), that had undergone similar thermal cycle, shows higher hardness (66VHN). This is expected due to typical grain refinement during thermo-mechanical processing in severe plastic deformation processes, such as AFS. Detailed microstructural investigation is being conducted to substantiate this result.

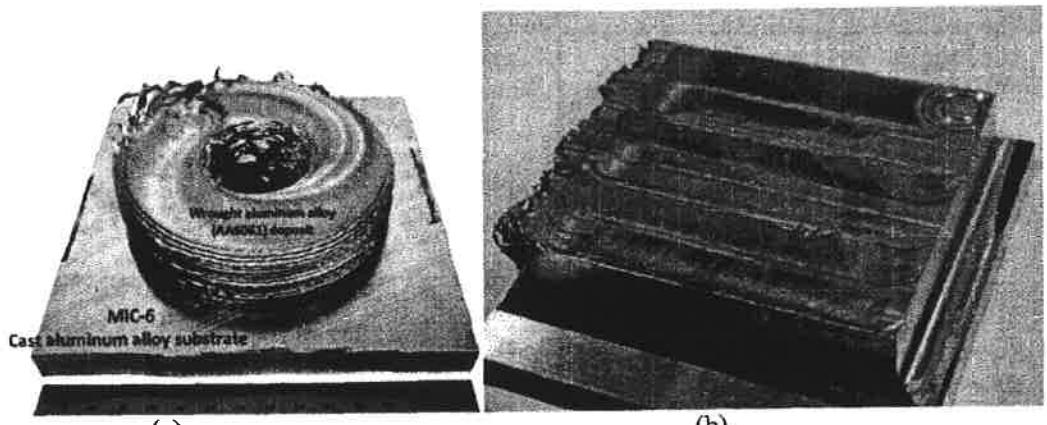

(a) (b)

Figure 3: Demonstration of AFS additive manufacturing a) 6 in. OD aluminum ring -18 layers of 6061Al on a MIC-6 cast plate, and b) 5 in. x 6in. Mg block with 30 layers of AZ31B on same substrate.

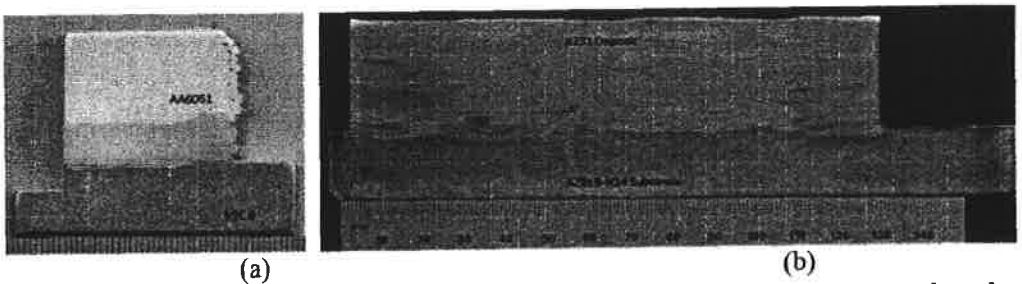

(a) (b)

Figure 4. Cross section of additively manufactured Al and Mg alloy structure show layered structure. a) Aluminum ring structure of AA6061, and b) Mg block of AZ31. Each division shown in scale is 1mm. The etching contrast difference in aluminum deposit is due to two different heats of 6061 filler, not due to dilution of substrate into the coating.

The tensile properties of the AFS-deposited 6061 ring and AZ31 plate are summarized in Table 2 and Table 3. The AFS-deposited material is subjected to the temperature above the solutionizing temperature of 6061 and the strengthening due to T6 is lost. The tensile strength of 6061-T6 was 287MPa; and after deposition the strength reduced to 120-150MPa. The tensile strength of solutionized AA6061-O is 124MPa [13] and the tensile strength of deposited metal matches with the strength of solutionized AA6061-O. Hence, it is possible to strengthen the deposited material to its full potential by post-deposit aging without requiring solutionizing. A detailed microstructural and post deposition heat treatment study is underway to confirm this hypothesis.

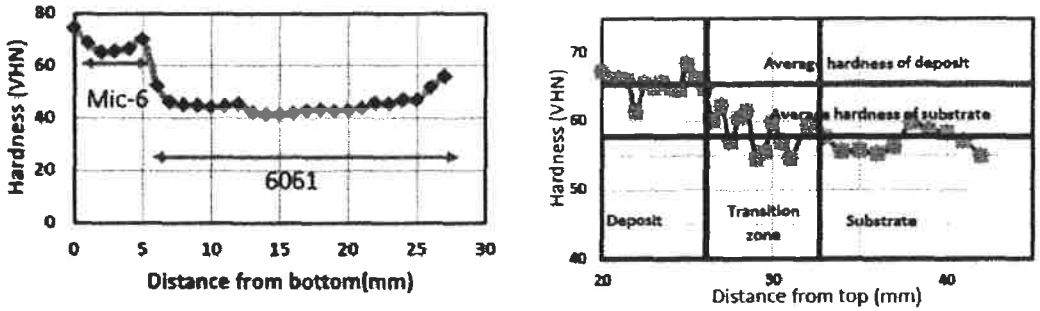

(a) (b)

Figure 5: Hardness profile along the thickness direction across the deposit/substrate interface. (a) AA6061 deposite on MIC-6, and b) AZ31 in AZ31.

Table 2. Table shows the summary of tensile properties of additively manufactured aluminum ring structure and the tensile sample orientation.

Sample ID	Tensile Strength (MPa)	Engineering Strain (%)
Base Metal (D13-D15)	140±7	3 ± 0
Filler metal	287±2	9±0
Deposit – Vertical 1 (D1-D3)	123±5	7±4
Deposit – Vertical 2 (D4-D6)	135±2	6±1
Deposit – Transverse (D7-D9)	141±10	13±1
Deposit – Longitudinal(D10-D12)	149±5	16±2

Table 3. Table shows the summary of tensile properties of additively manufactured magnesium block and the tensile sample orientation. L-Longitudinal, T-Transverse and ST-Short transverse.

Sample ID	Tensile Strength (MPa)	Engineering Strain (%)
Base Metal AZ31B-H24 (L)	264±1	20±1
Base Metal AZ31B-H24 (T)	267±2	19±3
Base Metal AZ31B-H24 (ST))	293±5	23±1
Deposit (L)	254±4	14±2
Deposit (T)	264±2	18±1
Deposit (ST)	333±2	19±1

The tensile properties of the as-deposited AZ31 block (Table 3) reveal that in work-hardened magnesium alloys, the loss of strength due to the thermal cycle of the process can be

compensated by grain refinement. The results show that tensile behavior of the substrate material is similar in the rolling and transverse directions. However, the tensile behavior is drastically different in the through-thickness/short transverse direction. This is expected to be the result of microstructural texture effect of HCP metal The yield strength of the substrate material was 175–190MPa, and tensile strength was 260-265MPa, with an average elongation of 20% in longitudinal and transverse directions. In the short transverse direction, the yield strength was 85MPa and the tensile strength was 290MPa. The tensile curve for the short transverse direction is shown in Figure 6, and is representative of a twin dominant tensile deformation behavior. The orientation of the microstructure with respect to the loading direction expected to favor tensile twinning in the short transverse direction rather than the slip-based deformation which is observed in the substrate and deposited materials in the longitudinal and transverse directions. The tensile strengths of deposits in the processing and transverse directions were comparable to that of the substrate even after being subjected to the large number of thermal cycles imparted due to deposition of 30 successive layers. It should be noted that the substrate was in the H24 work hardened condition. During AFS deposition, the filler metal is subjected to a thermal cycle which is expected to annihilate the work hardening effect. In deposited material, the grain refinement is expected to compensate the loss of work hardening due to thermal input during the deposition. However, in the thickness/short transverse direction, the tensile strength of the deposit was 40 MPa higher than the substrate. It is evident from the superimposed graphs of the substrate and deposit that the tensile strength of the deposit in the through-thickness direction is superior to the base metal while in other directions it is comparable. The elongation of the deposited material varied with direction: the maximum elongation (18%) was in the through-thickness direction and the minimum elongation (13%) was observed in the longitudinal direction. It is believed that the tensile properties of the AZ31 deposit can be further improved by lowering the heat input. The tensile behavior of both base and deposit are compared in Figure 6.

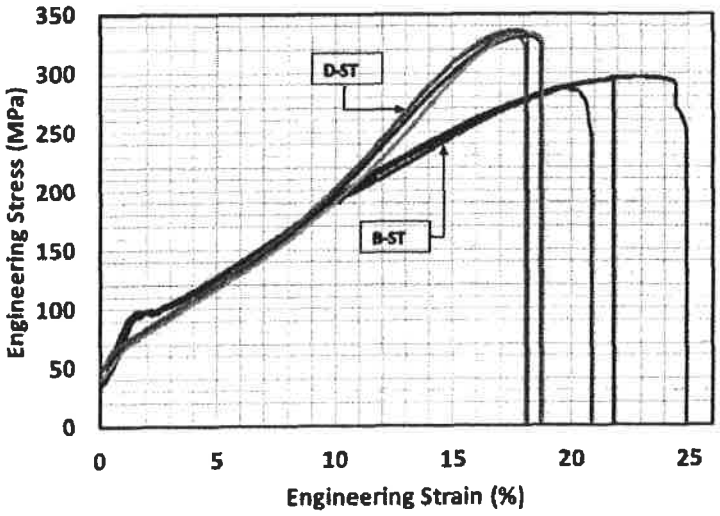

Figure 6: Comparison of short transverse direction tensile behavior of parent metal and deposited material.

Deposition of WE43 magnesium alloy powder

Test coupons fabricated from the WE43 powder, with intermittent stir procedure, were 2-4 inches in length and approximately 1.25 inches wide. The thickness of each pass was 0.063 inches thick and there were 6 passes in multiple pass deposition. The photographs of successful single pass and multi-pass deposits are shown in Figure 7. The process parameters used for these depositions were: 750rpm spindle speed; 1inch/min translation rate; and 0.6inch/min filler feed rate.

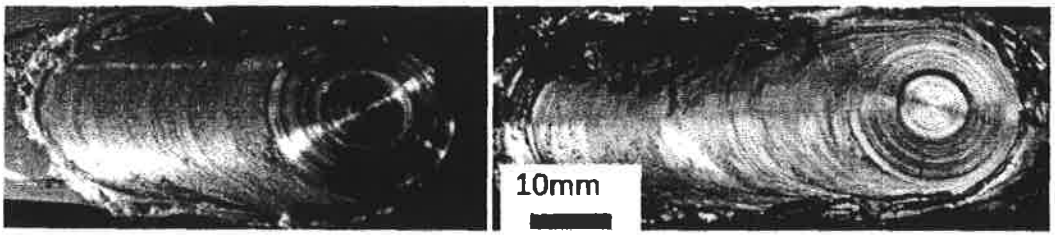

Figure 7: Photographs of successful single pass deposition (a), and multiple-pass deposition (b).

A macrograph of the multiple pass deposit is shown in Figure 8. The thickness of the deposit in the middle portion is about 7mm. As seen in the macrograph, the substrate, which is AZ31, deforms outward as the stronger WE43 material is being deposited onto it. It should be noted that WE43 possesses excellent high temperature properties, whereas AZ31 becomes very soft at the AFS processing temperature. This issue can be avoided by changing the substrate material to WE43 and using a wider substrate. This problem was successfully avoided when the similar base metal and filler metal were used. This can be seen in AFS-manufactured block of AZ31 on AZ31B-H24 substrate.

Figure 8: Macrograph of multiple pass WE43 deposit showing intermixed layer near the interface and uniform microstructure towards the top layer (each division is 1mm).

Figure 9a is an optical micrograph from the uniform region of the WE43 deposit shown above. The micrograph indicates that the grain size is fine, but a definitive size cannot be resolved using optical microscopy. The same sample was observed using SEM in backscattered electron mode and secondary electron mode, as shown in Figure 9b & c respectively. EBSD analysis is planned and expected to provide grain size details. The metallographic analysis confirms that the deposition is fully dense and the microstructure is uniform without any voids or any other defects.

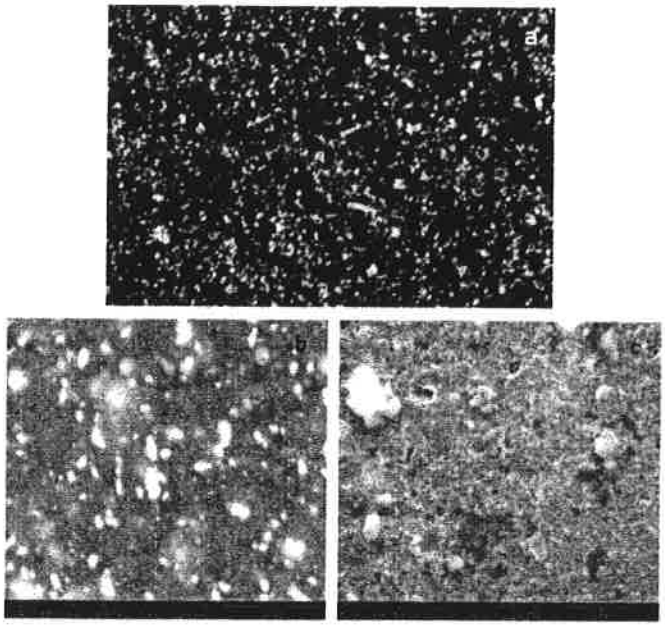

Figure 9: Micrographs of WE43 deposit from a) optical microscopy of b) SEM Back scattered electron image, and c) secondary electron image.

The SEM backscattered image shown in Figure 9b reveals about 0.5μm and smaller Y- and Nd-rich precipitates. The chemical composition of the precipitates was confirmed by EDS spot analysis, as shown in Table 4. In the same micrograph, finer particles are seen between the larger Y- and Nd-rich precipitates but a compositional analysis was not obtainable via EDS in the SEM. The secondary electron image shown in Figure 9c also does not reveal any additional information. The EDS spot analysis on the matrix (blue arrow) shows that the yttrium content is 1.4 atomic %, which is less than the yttrium content in the alloy. The depletion of yttrium in the matrix could be due to excessive precipitation during deposition or the preexistence of solute-rich precipitates in the powder. The existence of solute-rich precipitates in WE43 powder chipped from ingots was reported by Tandon et al. [14 & 15]. Further, they reported that these precipitates originate from the eutectic phase formed during the ingot manufacturing. If these larger precipitates existed in the powder, the AFS process has fractured them into smaller particles and dispersed them more evenly. Fracture and dispersion of large precipitates has been observed after AFS processing of cast scandium-rich aluminum ingots.

Table 4: Results of EDS spot analysis of powder deposited WE43.

Location	Mg	Y	Nd	
Blue	91.68	6.91	1.41	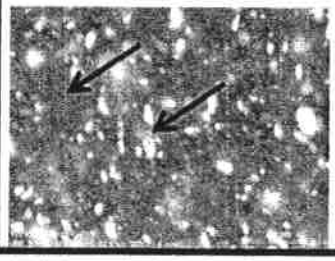
Red	98.21	1.47	0.32	

The mechanical properties of deposited WE43 are summarized in Figure 10a & b. The hardness profile across the deposit is uniform with a slight dip in the middle. The average hardness is 72.6±1.7 VHN, which is comparable to the hardness reported for solutionized and water-quenched WE43 [16]. Further heat treatment is expected to improve the hardness of the deposited materials. Tensile stress-strain curves are shown in Figure 10b for two representative miniature tensile samples extracted from the WE43 deposit. The average yield strength is 240MPa; the average tensile strength is 290MPa; the average elongation is 6%. Further, controlling the process parameters to reduce the heat input and extracting the heat by external means to increase the cooling rate is expected to favor further grain refinement and retaining the solute in the matrix. This aspect of the process improvement is expected to strengthen the deposit by Hall-Petch strengthening, solid solution strength and precipitation hardening.

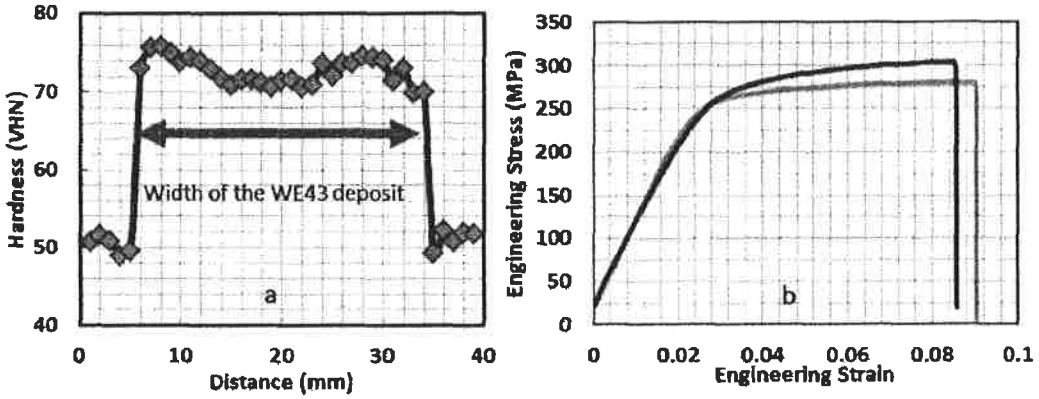

Figure 10: Mechanical properties of AFS WE43 powder deposit. (a) Hardness profile across the WE43 deposit shows an average hardness of 72.6±1.7VHN, and (b) Tensile behavior of WE43 deposit.

Conclusion

In this paper we have demonstrated capabilities of the AFS process as an additive manufacturing process for aluminum and magnesium alloys in solid and powder form. The following conclusions were derived.

- The mechanical properties of AFS deposited AA6061 in as deposited condition is comparable with solutionized condition.
- The mechanical properties of the AFS-deposited AZ31B were comparable to base metal in both the processing and transverse directions in as deposited condition.
- The tensile strength of the AFS-deposited AZ31-H24 was considerably higher than the base metal in the short transverse direction, and the through-thickness direction is typically the weakest direction in additive processes.
- The AFS process is capable of consolidating and depositing magnesium powders into fully dense, defect-free wrought structures with desirable mechanical properties.
- The mechanical properties of AFS-processed WE43 are considerably better than for powder-forged WE43 and comparable to heat treated wrought magnesium alloys.

References

1. http://energy.gov/articles/building-american-economy-last-american-competiveness-manufacturing.
2. http://www.ornl.gov/sci/manufacturing/docs/Aerospace_Workshop_Report.pdf
3. J.-P. Kruth, M.C. Leu and T. Nakagawa, Progress in additive manufacturing and rapid prototyping, CIRP Annals - Manufacturing Technology, 47 (2) (1998) 525-54.
4. E. Yasa, J-P. Kruth, Microstructural investigation of selective laser melting 316L stainless steel parts exposed to laser re-melting, Procedia Engineering, 19 (2011) 389-395.
5. V. K. Balla, P. D. DeVasConCellos, W. Xue, S. Bose and A. Bandyopadhyay Fabrication of compositionally and structurally graded Ti–TiO2 structures using laser engineered net shaping (LENS), Acta Biomaterialia, 5 (5) (2009) 1831-1837.
6. L.E. Murr, S.M. Gaytan, A. Ceylan, E. Martinez, J.L. Martinez, D.H. Hernandez, B.I. Machado, D.A. Ramirez, F. Medina, S. Collins, R.B. Wicker Characterization of titanium aluminide alloy components fabricated by additive manufacturing using electron beam melting, Acta Materialia, 58 (5) (2010) 1887-1894.
7. V. D. Fachinotti, A. Cardona, B. Baufeld and O. Van der Biest, Finite-element modelling of heat transfer in shaped metal deposition and experimental validation, Acta Materialia, 60 (19) (2012) 6621-6630.
8. D. Seo, K. Ogawa, K. Sakaguchi, N. Miyamoto, Y. Tsuzuki, Parameter study influencing thermal conductivity of annealed pure copper coatings deposited by selective cold spray processes, Surface and Coatings Technology, 206 (8–9) (2012) 2316-2324.
9. T. Shamim, C. Xia and P. Mohanty, Modeling and analysis of combustion assisted thermal spray processes, International Journal of Thermal Sciences, 46 (8) (2007) 755-767.
10. R.R. Dehoff, S.S. Babu, Characterization of interfacial microstructures in 3003 aluminum alloy blocks fabricated by ultrasonic additive manufacturing Acta Materialia, 58 (13) (2010) 4305-431.
11. R.S. Mishra and Z.Y. Ma, Friction stir welding and processing, Materials Science and Engineering: R: Reports, 50 (1–2) (2005) 1-78.
12. J. J. S. Dilip, S. Babu, R. S. Varadha, K. H. Rafi, G.D. Janaki Ram and B. E. Stucker, Use of Friction Surfacing for Additive Manufacturing, MATERIALS AND MANUFACTURING PROCESSES, 28 (2) (2013) 189-194.
13. ASM handbooks online, Volume 2, Properties and Selection: Nonferrous Alloys and Special-Purpose Materials -> Properties of Wrought Aluminum and Aluminum Alloys -> 6061 Alclad 6061.
14. R. Tandon, D. Madan, J. McConaghie, D. Kapoor and K. Cho Influence of Powder Characteristics on the Consolidation Behavior of Magnesium Alloys for Structural and Energetic Applications, The 2012 International Conference on Powder Metallurgy & Particulate Materials, June 10-13, 2012; Nashville, TN.
15. R. Tandon, D. Madan, J. McConaghie, J. Paras, D. Kapoor and K. Cho The 2011 International Conference on Powder Metallurgy & Particulate Materials, May 18-21; San Francisco, CA
16. G. Riontino et al., A novel thermal treatment on a Mg–4.2Y–2.3Nd–0.6Zr (WE43) alloy, Materials Science and Engineering A, 494 (2008) 445–44.